Available online at www.sciencedirect.com
SCIENCE DIRECT®
ELSEVIER
International Journal of Solids and Structures 42 (2005) 5513–5535
INTERNATIONAL JOURNAL OF SOLIDS and STRUCTURES
www.elsevier.com/locate/ijsolstr

A boundary value method for the singular behavior of bimaterial systems under inplane loading

Xiao Gui Wang *

College of Mechanical Engineering, Zhejiang University of Technology, Zhaohui Liu Section, Hangzhou 310014, PR China

Received 22 November 2004; received in revised form 18 February 2005
Available online 7 April 2005

Abstract

Based on the governing equations of linear elasticity, this paper develops a novel boundary value method to study the singular behavior of elastic stress fields at the corners of bimaterial wedges and junctions by using the eigenfunction expansion technique. The resulted one-dimensional differential system, which consists of the reduced equilibrium equations and boundary conditions, just relates to an angular coordinate in the polar coordinate system. Implementing discretization of this differential system by the finite cloud method, we readily derive the so-called generalized eigenproblem in the singular eigenvalue. The performance of the methodology is subsequently verified through the well-known crack and interface crack problems, demonstrating high accuracy and quick convergence characteristics. In addition, a selected set of practically useful models is numerically analyzed to examine the angular variations of the displacement and stress fields, and the influences of wedge-side boundary conditions to singular behavior are also studied.

Keywords: Boundary value; Characteristic equation; Singularity; Bimaterial system

1. Introduction

It is very well documented that the conventional materials do not have the ability to provide the particular requirements of reinforcement, such as the stronger, the harder, the tougher, the lighter and etc., for the striking development of modern industry. Because the properties can be tailored to suit these

* Tel.: +86 571 81857006; fax: +86 571 88320130.
E-mail address: mechwxg@yahoo.com.cn

0020-7683/$ - see front matter © 2005 Elsevier Ltd. All rights reserved.
doi:10.1016/j.ijsolstr.2005.02.039

particular requirements, the composites created by the deliberate combination of multiple dissimilar materials are extensively employed in modern industrial spheres. Although the reinforced composites have the excellent properties applicable to specified engineering applications, their bonding interfaces near the free wedge surface or the junction corner inevitably suffer high stress gradients (stress singularities) due to the mismatches of elasticity and geometry, which may lead to the crack initiation being the precondition for the failure of structures. Therefore, the comprehensive understanding of singular behavior of multi-material junctions and wedges plays the most crucial role in the optimum design and failure analysis of such systems.

Many researchers have investigated the singular behavior of bonded dissimilar materials with various methods. The study starts from the pioneering work of Williams (1959) who use the eigenfunction expansion technique to analyze the stress singularity of the interface crack problem. Using the Mellin transform method, Bogy (1971) studies the order of stress singularity and the related displacement and singular stress fields at the vicinity of the interface wedge of bonded dissimilar materials in plane elasticity problems. On the other hand, Bogy and Wang (1971) and Chen and Nisitani (1993) investigate the singular behavior of the interface corner problems by Mellin transform method and complex function method, respectively. Recently, Chen et al. (2002, 2003, 2004) study the interaction problems of a dislocation and a crack based on the complex variable method. The previous asymptotic analysis of stress singularity tells us one fact that the displacement solutions take to be of the form $r^s f(\theta)$ in a polar coordinate system (r,θ) originated from the singular point. However, these analytical solutions on the characteristic equation for determining the orders of the stress singularity and the angular variations of displacement and singular stress fields are restricted to a very few specifically geometrical configurations and material combinations. For the complex problems of bonded materials, the derivation of the explicit solutions appears to be very difficult even though with outstanding mathematical competence. Fortunately, the numerical method, such as the boundary element method (Liang and Liew, 2001; Xu et al., 2001; Liew and Liang, 2002, 2003) and the finite element method, can serve as an advisable and appropriate choice to be resorted to. Bazant and Estenssoro (1979), Somaratna and Ting (1986), Ghahremani (1991) and Gu and Belytschko (1994) develop a finite element procedure based on the weak form of the variational principle to extract the three-dimensional stress singularity. Sze and Wang (2000) propose another finite element formulation by using the weak form of the governing equations for computing the stress singularities at bimaterial interfaces. Pageau et al. (1995) extends the sectorial finite element which is devised by Yamada and Okumura (1983) based on the virtual work principle and singular transformation technique to the singularity analysis of anisotropic materials. All of these finite element methods result in a linear characteristic matrix equation whose physically admissible eigenvalues and associated eigenvectors of the analytical models correspond to the singularity orders and the angular variations of displacement field in the dominant field of stress singularity, respectively. In addition, Xu et al. (1999) presents a numerical model to determine multiple singularities and related stress intensity factors starting with the asymptotic stress field and the common numerical results obtained by the boundary element procedure.

In this paper, a novel boundary value method is developed based on the governing equations of linear elasticity for computing the orders of stress singularity and the associated angular variations of displacement and singular stress fields for bimaterial systems under inplane loading. The discretization of the resulting one-dimensional governing differential system, making up of the reduced equilibrium equations and the boundary conditions, are accomplished by the finite cloud method (Aluru and Li, 2001). Consequently, the linear characteristic matrix equation about the singular eigenvalues is derived and then solved numerically by the LAPACK subroutine. The computed results of the well-known crack and interface crack problems verify the convergence and accuracy characteristics of the present method. Finally, the methodology is applied to a selected set of practically useful bimaterial wedges and junctions to study the singular behavior of the interface edge.

2. Governing equations

2.1. The basic equations of linear elasticity

In terms of the unknown displacement functions u and w, the fundamental partial differential equations governing the mechanical equilibrium of the homogeneous isotropic elastic body in plane strain or plane stress, with reference to a polar coordinate system (r,θ), take the form

$$\begin{aligned}&(\lambda+2\mu)\left(\frac{\partial^2 u}{\partial r^2}+\frac{1}{r}\frac{\partial u}{\partial r}-\frac{u}{r^2}\right)+\frac{\mu}{r^2}\frac{\partial^2 u}{\partial\theta^2}+\frac{\lambda+\mu}{r}\frac{\partial^2 w}{\partial r\partial\theta}-\frac{\lambda+3\mu}{r^2}\frac{\partial w}{\partial\theta}=0\\&\frac{\lambda+\mu}{r}\frac{\partial^2 u}{\partial r\partial\theta}+\frac{\lambda+3\mu}{r^2}\frac{\partial u}{\partial\theta}+\mu\left(\frac{\partial^2 w}{\partial r^2}+\frac{1}{r}\frac{\partial w}{\partial r}-\frac{w}{r^2}\right)+\frac{\lambda+2\mu}{r^2}\frac{\partial^2 w}{\partial\theta^2}=0\end{aligned}\tag{1}$$

in the absence of body forces. Furthermore, the strain–displacement relations

$$\begin{aligned}\varepsilon_r&=\frac{\partial u}{\partial r}\\\varepsilon_\theta&=\frac{u}{r}+\frac{1}{r}\frac{\partial w}{\partial\theta}\\\gamma_{r\theta}&=\frac{1}{r}\frac{\partial u}{\partial\theta}+\frac{\partial w}{\partial r}-\frac{w}{r}\end{aligned}\tag{2}$$

and the linear constitutive equations

$$\begin{aligned}\sigma_r&=(\lambda+2\mu)\varepsilon_r+\lambda\varepsilon_\theta\\\sigma_\theta&=\lambda\varepsilon_r+(\lambda+2\mu)\varepsilon_\theta\\\sigma_{r\theta}&=\mu\gamma_{r\theta}\end{aligned}\tag{3}$$

where u, ε_r and σ_r are the components of displacement, strain and stress along the radial direction, respectively; w, ε_θ and σ_θ are the components of displacement, strain and stress along the circumferential direction, respectively; $\gamma_{r\theta}$ is the shear strain and $\sigma_{r\theta}$ is the shear stress; and λ, μ are known as the Lame elastic constants. The partial differential equations of equilibrium (1) together with the prescribed Neumann and Dirichlet boundary conditions can completely determine the two fundamental variables u and w, and by invoking of which the components of strain and stress are obtained directly from the strain–displacement relations (2) and linear constitutive equations (3).

2.2. Bimaterial systems

The bimaterial systems can be separated into two cases: bimaterial junction and bimaterial wedge as illustrated in Fig. 1, with E_j, v_j and Ω_j $(j=1,2)$ denoting the Young's modulus, Poisson's ratio and the occupied region of the respective homogeneous isotropic elastic materials. The bonded dissimilar materials couple to each other through the interface continuity conditions of the displacements and tractions, out of question, which are regarded as the key ingredient for determining the stress singularity introduced by the elastic mismatches. In addition, the effects of the geometrical configuration and the boundary conditions at the wedge-side surfaces should be also considered.

The interface continuity conditions of the displacements and tractions have the unique forms at the interface $\theta=\theta_0$,

$$u^{(1)}(r,\theta_0)=u^{(2)}(r,\theta_0)\quad w^{(1)}(r,\theta_0)=w^{(2)}(r,\theta_0)\tag{4a}$$

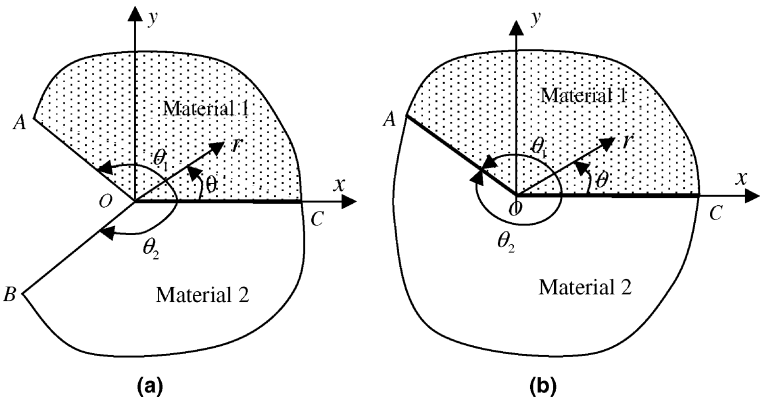

Fig. 1. Geometry and coordinate definitions for the bonded bimaterial systems: (a) bimaterial wedge; (b) bimaterial junction.

$$\sigma_\theta^{(1)}(r,\theta_0)=\sigma_\theta^{(2)}(r,\theta_0)\quad \sigma_{r\theta}^{(1)}(r,\theta_0)=\sigma_{r\theta}^{(2)}(r,\theta_0) \tag{4b}$$

where the superscripts (1) and (2) denote the corresponding components in the regions Ω_1 and Ω_2, respectively. However, for the boundary conditions at the two wedge-side surfaces such as $\theta=\theta_1$ and $\theta=\theta_2$, there are three physically admissible cases according to the arbitrary combinations of traction-free and displacement-clamped, i.e.

(1) Traction-free and traction-free (TT)

$$\sigma_\theta^{(1)}(r,\theta_1)=\sigma_{r\theta}^{(1)}(r,\theta_1)=\sigma_\theta^{(2)}(r,\theta_2)=\sigma_{r\theta}^{(2)}(r,\theta_2)=0 \tag{5a}$$

(2) Traction-free and displacement-clamped (TD)

$$\sigma_\theta^{(1)}(r,\theta_1)=\sigma_{r\theta}^{(1)}(r,\theta_1)=0\quad u^{(2)}(r,\theta_2)=w^{(2)}(r,\theta_2)=0 \tag{5b}$$

(3) Displacement-clamped and displacement-clamped (DD)

$$u^{(1)}(r,\theta_1)=w^{(1)}(r,\theta_1)=u^{(2)}(r,\theta_2)=w^{(2)}(r,\theta_2)=0 \tag{5c}$$

If the wedge angles θ_1 and θ_2 are both equal to 180°, we obtain the famous interface crack model.

2.3. Asymptotic forms of the basic equations

It is well known from the available analytical and numerical studies that, due to the specifically geometrical configurations such as a crack or/and the elastic mismatch across the interface of the bonded dissimilar materials, the displacement and singular stress fields with the exponent singularities at the vicinity of the vertex points (such as the interface edge, interface corner and the tip of the interface crack) are proportional to certain power of the distance from those points. In general, the singular stress field takes to be of the asymptotic form, which can be constructed easily provided that the homogeneous solutions of displacement field are expressed on the basis of separation of variables by

$$u(r,\theta)=r^s\Lambda_r(\theta)\quad w(r,\theta)=r^s\Lambda_\theta(\theta) \tag{6}$$

where $\Lambda_r(\theta)$ and $\Lambda_\theta(\theta)$ represent the angular variations of displacement components, and s is the singular eigenvalue. In this paper, only the values in the range $0<\mathrm{Re}(s)<1$ are considered because of two reasons. One is that, for the purpose of occurring stress singularities at the apex, the condition $\mathrm{Re}(s)<1$ should be

satisfied. Another is $\mathrm{Re}(s) > 0$ to ensure that both the displacements and elastic strain energy are bounded. Substituting (6) into the constitutive equations (3), gives

$$\left\{\begin{array}{c}\sigma_r(r,\theta)\\ \sigma_\theta(r,\theta)\\ \sigma_{r\theta}(r,\theta)\end{array}\right\} = r^{s-1}\left\{\begin{array}{c}\Sigma_r(\theta)\\ \Sigma_\theta(\theta)\\ \Sigma_{r\theta}(\theta)\end{array}\right\} = r^{s-1}\left(\left[\begin{array}{cc}\lambda+2\mu & 0\\ \lambda & 0\\ 0 & \mu\end{array}\right]s + \left[\begin{array}{cc}\lambda & \lambda\cdot\frac{\partial}{\partial\theta}\\ \lambda+2\mu & (\lambda+2\mu)\cdot\frac{\partial}{\partial\theta}\\ \mu\cdot\frac{\partial}{\partial\theta} & -\mu\end{array}\right]\right)\left\{\begin{array}{c}\Lambda_r(\theta)\\ \Lambda_\theta(\theta)\end{array}\right\} \tag{7}$$

And then, substituting of Eq. (6) into (1) and eliminating the common factor r^{s-2} from both sides, the reduced differential equations of equilibrium just with respect to the angular coordinate θ are given by

$$a_k s^2 + b_k s + c_k = 0 \quad (k = 1, 2) \tag{8}$$

where

$$\begin{aligned} a_1 &= (\lambda+2\mu)\Lambda_r(\theta)\\ a_2 &= \mu\Lambda_\theta(\theta)\\ b_1 &= (\lambda+\mu)\Lambda'_\theta(\theta)\\ b_2 &= (\lambda+\mu)\Lambda'_r(\theta)\\ c_1 &= \mu\Lambda''_r(\theta) - (\lambda+2\mu)\Lambda_r(\theta) - (\lambda+3\mu)\Lambda'_\theta(\theta)\\ c_2 &= (\lambda+3\mu)\Lambda'_r(\theta) - \mu\Lambda_\theta(\theta) + (\lambda+2\mu)\Lambda''_\theta(\theta) \end{aligned} \tag{9}$$

In Eq. (9) and in the following sections, the single prime ($'$) and the double prime ($''$) respectively denote the first and second derivatives of the imposed quantities unless otherwise specially stated. Similarly, the reduced interface continuity conditions and the reduced boundary conditions can be easily obtained from Eqs. (4) and (5).

Up to now, a one-dimensional boundary value problem for determining the singular behavior of the bimaterial systems is constructed, which consists of the reduced forms of the prescribed interface continuity conditions, the boundary conditions at the wedge-side surfaces, and the equilibrium equations to be satisfied at all points in the interior of the region.

3. Singularity characteristic equations

3.1. Formulation discretization

The finite cloud method (FCM), which combines collocation with the fixed reproducing kernel technique, is introduced to construct the meshless point interpolation functions for the discretization of the boundary value problem outlined in the preceding section. This numerical algorithm uses a corrected kernel to generate an approximation to the unknown continuous function. As an example, the discrete form of the approximation for the one-dimensional function $f(x)$ is given by

$$f(x) = \sum_{j=1}^{n} N_j(x, x_k)\tilde{f}_j \tag{10}$$

where n is the total number of scattered points in the computational domain occupied by the materials, x_k is any point in the domain at which the fixed kernel function is centred, $\tilde{f}_j$ is the unknown nodal value associated with node j, and the interpolation function $N_j(x, x_k)$ centred at x_k with respect to node j is defined as

$$N_j(x, x_k) = \mathbf{P}^{\mathrm{T}}(x)\mathbf{Q}^{-1}(x_j, x_k)\mathbf{P}(x_j)K(x_k - x_j)\Delta V_j \tag{11}$$

where ΔV_j is a measure of the domain surrounding the node j, $K(x_k - x_j)$ is the uncorrected kernel function, $\mathbf{Q}(x_j, x_k)$ is a symmetric constant matrix of correction function coefficients, and $\mathbf{P}(x)$ is the vector of basis function. In this paper, the quadratic basis

$$\mathbf{P}(x) = [1, x, x^2]^{\mathrm{T}} \tag{12}$$

and the cubic spline for the kernel function

$$K(x_k - x_j) = \frac{1}{d}\begin{cases} 0 & 2 < z_j \\ (2 - z_j)^3/6 & 1 \leqslant z_j \leqslant 2 \\ (2/3) - z_j^2(1 - z_j/2) & 0 \leqslant z_j \leqslant 1 \end{cases} \tag{13}$$

are adopted, where $z_j = |(x_k - x_j)/d|$ with d denoting the cloud size in the x-direction.

For the previously derived one-dimensional boundary value problem, the angular variations of displacement fields are treated as the fundamental variables, whose approximated values and derivatives located at the interior scattered point k are given by the FCM interpolation functions as follows:

$$\Lambda_r(\theta_k) = \sum_{j=1}^{n} N_j(\theta_k)\tilde{u}_j \quad \Lambda_\theta(\theta_k) = \sum_{j=1}^{n} N_j(\theta_k)\tilde{w}_j \tag{14}$$

and

$$\begin{aligned} \Lambda_r'(\theta_k) &= \sum_{j=1}^{n} N_j'(\theta_k)\tilde{u}_j \quad \Lambda_\theta'(\theta_k) = \sum_{j=1}^{n} N_j'(\theta_k)\tilde{w}_j \\ \Lambda_r''(\theta_k) &= \sum_{j=1}^{n} N_j''(\theta_k)\tilde{u}_j \quad \Lambda_\theta''(\theta_k) = \sum_{j=1}^{n} N_j''(\theta_k)\tilde{w}_j \end{aligned} \tag{15}$$

where $\tilde{u}_j$ and $\tilde{w}_j$ are the unknown nodal displacement angular variations, and θ_k is the angular coordinate of node k. It should be pointed out that the interpolation function $N_j(x, x_k)$ has been rewritten into the more concise expression as $N_j(x_k)$ for simplicity, and this rule is also applicable to the derivatives.

Substituting Eqs. (14) and (15) into (7), the discrete approximations of the angular variations of stress components at the node k are represented as

$$\begin{Bmatrix} \Sigma_r(\theta_k) \\ \Sigma_\theta(\theta_k) \\ \Sigma_{r\theta}(\theta_k) \end{Bmatrix} = \left(s\begin{bmatrix} (\lambda + 2\mu)\mathbf{N}(\theta_k) & 0 \\ \lambda\mathbf{N}(\theta_k) & 0 \\ 0 & \mu\mathbf{N}(\theta_k) \end{bmatrix} + \begin{bmatrix} \lambda\mathbf{N}(\theta_k) & \lambda\mathbf{N}'(\theta_k) \\ (\lambda + 2\mu)\mathbf{N}(\theta_k) & (\lambda + 2\mu)\mathbf{N}'(\theta_k) \\ \mu\mathbf{N}'(\theta_k) & -\mu\mathbf{N}(\theta_k) \end{bmatrix} \right) \begin{Bmatrix} \tilde{\mathbf{u}} \\ \tilde{\mathbf{w}} \end{Bmatrix} \tag{16}$$

where $\tilde{\mathbf{u}}$ and $\tilde{\mathbf{w}}$ are the column vectors with a size of n for the respective unknown nodal angular variations of displacement components $\tilde{u}_j$ and $\tilde{w}_j$, and $\mathbf{N}(\theta_k)$ is the row vector with a size of n for the interpolation function. In the same manner, the discrete approximations of the reduced differential equations of equilibrium (8) corresponding to each scattered points of the whole computational domain are easily given in the matrix forms

$$\left(\begin{bmatrix} \mathbf{A}_{uu} & \mathbf{A}_{uw} \\ \mathbf{A}_{wu} & \mathbf{A}_{ww} \end{bmatrix} s^2 + \begin{bmatrix} \mathbf{B}_{uu} & \mathbf{B}_{uw} \\ \mathbf{B}_{wu} & \mathbf{B}_{ww} \end{bmatrix} s + \begin{bmatrix} \mathbf{C}_{uu} & \mathbf{C}_{uw} \\ \mathbf{C}_{wu} & \mathbf{C}_{ww} \end{bmatrix} \right) \begin{bmatrix} \tilde{\mathbf{u}} \\ \tilde{\mathbf{w}} \end{bmatrix} = 0 \tag{17}$$

where the entries of the coefficient-submatrix $\mathbf{A}_{pq}$, $\mathbf{B}_{pq}$ and $\mathbf{C}_{pq}$ $(p, q = u, w)$ with a size of n by n are given the Appendix A. Eq. (17) must be satisfied at all scattered points throughout the whole volume of the considered body except those points located at the material or geometrical boundaries, whereon the Neumann and Dirichlet boundary conditions are prescribed.

3.2. Semi-infinite crack

For the model of a semi-infinite crack in the isotropic material, by the means of (16), the discrete approximations of the *Traction-free* boundary conditions on the crack surface can be rewritten into the matrix forms as follows

$$\left(\begin{bmatrix} \mathbf{b}_{uu} & \mathbf{0} \\ \mathbf{0} & \mathbf{b}_{ww} \end{bmatrix} s + \begin{bmatrix} \mathbf{c}_{uu} & \mathbf{c}_{uw} \\ \mathbf{c}_{wu} & \mathbf{c}_{ww} \end{bmatrix} \right) \begin{bmatrix} \tilde{\mathbf{u}} \\ \tilde{\mathbf{w}} \end{bmatrix} = 0 \tag{18}$$

where the elements $\mathbf{b}_{pq}$ and $\mathbf{c}_{pq}$ with size of n are the row vectors and whose detailed entries are listed in Appendix B. In the same way, the discrete approximations of the *Displacement-clamped* boundary conditions on the crack surface are readily obtained

$$\begin{bmatrix} \mathbf{c}_{uu} & \mathbf{0} \\ \mathbf{0} & \mathbf{c}_{ww} \end{bmatrix} \begin{bmatrix} \tilde{\mathbf{u}} \\ \tilde{\mathbf{w}} \end{bmatrix} = 0 \tag{19}$$

where

$$[\mathbf{c}_{uu}]_j = [\mathbf{c}_{ww}]_j = N_j(\theta) \tag{20}$$

And then, by invoking of the combinations of Eqs. (18) and (19), we find the discrete approximations of the three physically admissible boundary conditions on two opposite surfaces of the crack.

In virtue of the finite cloud method, the final discrete representations of the reduced differential equations of equilibrium and the boundary conditions are derived by now. Prior to solving this boundary value problem, the boundary conditions prescribed on the nodes located at the two surfaces of the crack should be incorporated into the equilibrium equations. The actual implementation process of incorporation is efficiently carried out just by replacing the corresponding rows of the equilibrium equations in matrix form by the specified boundary conditions. Consequently, the so-called generalized eigenproblem nonlinear in the eigenvalue s is obtained

$$(\mathbf{A}s^2 + \mathbf{B}s + \mathbf{C}) \cdot \mathbf{x} = 0 \tag{21}$$

On account of incorporating the boundary conditions, the matrix $\mathbf{A}$ is singular. As a result, the characteristic equation (21) can be uniquely turned into the standard eigenproblem linear in the eigenvalue ω, with double sizes of the initial eigensystem, by introducing an additional unknown eigenvector $\mathbf{y}$

$$\begin{bmatrix} \mathbf{0} & \mathbf{I} \\ -\mathbf{C}^{-1}\mathbf{A} & -\mathbf{C}^{-1}\mathbf{B} \end{bmatrix} \cdot \begin{bmatrix} \mathbf{x} \\ \mathbf{y} \end{bmatrix} = \mathbf{D} \cdot \begin{bmatrix} \mathbf{x} \\ \mathbf{y} \end{bmatrix} = \omega \cdot \begin{bmatrix} \mathbf{x} \\ \mathbf{y} \end{bmatrix} \tag{22}$$

where

$$\omega = s^{-1} \quad \mathbf{x} = [\tilde{\mathbf{u}} \quad \tilde{\mathbf{w}}]^{\mathrm{T}} \quad \mathbf{y} = \omega\mathbf{x} \tag{23}$$

The characteristic equation is then solved numerically by the LAPACK subroutine to obtain our expected physically admissible eigenvalues and the associated eigenvectors.

3.3. Bimaterial systems

In the case of the bimaterial systems, such as the bimaterial wedge and bimaterial junction, each domain occupied by different materials must be approximated with its own point distribution. It should be noted that the pair of scattered points located on the specified interface have the same coordinates but belong to different point distributions. Let n_k denote the total number of scattered points within the computational domain Ω_k . Implementing the FCM to the reduced displacement interface continuity conditions, yields

$$\begin{bmatrix} \mathbf{c}_{uu}^{(1)} & \mathbf{0} & -\mathbf{c}_{uu}^{(2)} & \mathbf{0} \\ \mathbf{0} & \mathbf{c}_{ww}^{(1)} & \mathbf{0} & -\mathbf{c}_{ww}^{(2)} \end{bmatrix} \begin{bmatrix} \mathbf{x}^{(1)} \\ \mathbf{x}^{(2)} \end{bmatrix} = 0 \tag{24}$$

where $\mathbf{c}_{uu}^{(k)}$ and $\mathbf{c}_{ww}^{(k)}$ are the row vectors and $\mathbf{x}^{(k)}$ $(k = 1, 2)$ is the column vector with a size of n_k, and the entries of $\mathbf{c}_{uu}^{(k)}$ and $\mathbf{c}_{ww}^{(k)}$ have the same forms as Eq. (20) except that the interpolation functions are constructed in the respective point distribution. Similarly, implementing the FCM to the reduced traction interface continuity conditions, we have

$$\left(\begin{bmatrix} \mathbf{b}_{uu}^{(1)} & \mathbf{0} & -\mathbf{b}_{uu}^{(2)} & \mathbf{0} \\ \mathbf{0} & \mathbf{b}_{ww}^{(1)} & \mathbf{0} & -\mathbf{b}_{ww}^{(2)} \end{bmatrix} s + \begin{bmatrix} \mathbf{c}_{uu}^{(1)} & \mathbf{c}_{uw}^{(1)} & -\mathbf{c}_{uu}^{(2)} & -\mathbf{c}_{uw}^{(2)} \\ \mathbf{c}_{wu}^{(1)} & \mathbf{c}_{ww}^{(1)} & -\mathbf{c}_{wu}^{(2)} & -\mathbf{c}_{ww}^{(2)} \end{bmatrix} \right) \begin{bmatrix} \mathbf{x}^{(1)} \\ \mathbf{x}^{(2)} \end{bmatrix} = 0 \tag{25}$$

where $\mathbf{b}_{pq}^{(k)}$ and $\mathbf{c}_{pq}^{(k)}$ are the row vectors with a size of n_k whose entries have the same forms as those listed in Appendix B except that the domain occupied by different material has the respective elastic constants and interpolation functions are constructed in its own point distribution. Finally, implementing the FCM to the reduced differential equations of equilibrium (8) for the bimaterial systems, we find

$$\left(\begin{bmatrix} \mathbf{A}^{(1)} & \mathbf{0} \\ \mathbf{0} & \mathbf{A}^{(2)} \end{bmatrix} s^2 + \begin{bmatrix} \mathbf{B}^{(1)} & \mathbf{0} \\ \mathbf{0} & \mathbf{B}^{(2)} \end{bmatrix} s + \begin{bmatrix} \mathbf{C}^{(1)} & \mathbf{0} \\ \mathbf{0} & \mathbf{C}^{(2)} \end{bmatrix} \right) \begin{bmatrix} \mathbf{x}^{(1)} \\ \mathbf{x}^{(2)} \end{bmatrix} = 0 \tag{26}$$

where $\mathbf{A}^{(k)}$, $\mathbf{B}^{(k)}$ and $\mathbf{C}^{(k)}$ are the matrices with a size of $2n_k$ by $2n_k$ whose entries can be constructed in the same matter as Eq. (17) for each domain but with the previously mentioned exceptions.

What to do next is to incorporate the boundary conditions and the interface continuity conditions of displacements and tractions into the reduced differential equations of equilibrium. For the fully bonded bimaterial junction, only the interface continuity conditions along the two perfectly bonded interfaces (such as $\theta = 0$ and $\theta = \theta_1$) are considered, which are used to replace the *eight* reduced equilibrium equations corresponding to those scattered point located at the specified interface to accomplish the incorporating process. While for the bimaterial wedge and debonded bimaterial junction, the boundary conditions at the wedge-side surfaces (such as $\theta = \theta_1$ and $\theta = \theta_2$) besides the interface continuity conditions along the interface (such as $\theta = 0°$) should also be taken into account, and the similar replacement technique is carried out. Consequently, the so-called generalized eigenproblem is obtained, which can be readily transformed into the final standard eigenproblem.

3.4. The displacement and singular stress fields

Consider the characteristic matrix equation (22) of the real square matrix **D**. Any solution to the characteristic equation is an eigenvalue of **D** corresponding to at least one eigenvector. Note that matrix **D** is nonsymmetric, the physically admissible singular eigenvalues and the associated eigenvectors may be either real or conjugate complex. Without loss of generality, one representative case that the singular eigenvalues are two real or a pair of conjugate complex numbers, namely the case with two real or oscillatory singularities, is considered to study the displacement and singular stress fields in the vicinity of the singular point.

3.4.1. Two real singularities

In the case of the singular stress fields with two real singularities, the discrete displacement and singular stress components at the scattered meshless points θ_k can be represented in the summation form as following

$$\begin{aligned} u(r, \theta_k) &= r^{s_1} K_{\mathrm{I}} \Lambda_r^{\mathrm{I}}(\theta_k) + r^{s_2} K_{\mathrm{II}} \Lambda_r^{\mathrm{II}}(\theta_k) \\ w(r, \theta_k) &= r^{s_1} K_{\mathrm{I}} \Lambda_\theta^{\mathrm{I}}(\theta_k) + r^{s_2} K_{\mathrm{II}} \Lambda_\theta^{\mathrm{II}}(\theta_k) \end{aligned} \tag{27}$$

and

$$\sigma_{\alpha\beta}(r,\theta_k) = r^{s_1-1}K_{\mathrm{I}}\Sigma^{\mathrm{I}}_{\alpha\beta}(\theta_k) + r^{s_2-1}K_{\mathrm{II}}\Sigma^{\mathrm{II}}_{\alpha\beta}(\theta_k) \quad (\alpha,\beta = r,\theta) \tag{28}$$

where K_{I} and K_{II} denote the stress intensity factors for mode I and II respectively. The angular variations $\Lambda^j_\alpha(\theta_k)$ and $\Sigma^j_{\alpha\beta}(\theta_k)$ relate to the computed eigenvectors through Eqs. (14) and (16), respectively. Furthermore, the displacement and singular stress components between two adjacent meshless points can be readily obtained by means of the interpolation method. In order to compare the numerical results with the available explicit analytical solutions, it is worthwhile to normalize the angular variations $\Lambda^j_\alpha(\theta)$ and $\Sigma^j_{\alpha\beta}(\theta)$ by an identical rule Ξ_j. Applying the rule to Eqs. (27) and (28), we then have the displacement and singular stress fields with the specifically normalized angular variations.

3.4.2. Oscillatory singularities

In this case, the relevant quantities to the displacement and singular stress fields, including $\Lambda^j_\alpha(\theta)$, $\Sigma^j_{\alpha\beta}(\theta)$, s_j and K_j, are pairs of conjugate complex numbers, i.e.

$$\begin{aligned}
&\Lambda^{\mathrm{I}}_r(\theta) = \overline{\Lambda^{\mathrm{II}}_r(\theta)} = \Lambda^{\mathrm{Re}}_r(\theta) - \mathrm{i}\Lambda^{\mathrm{Im}}_r(\theta)\\
&\Lambda^{\mathrm{I}}_\theta(\theta) = \overline{\Lambda^{\mathrm{II}}_\theta(\theta)} = \Lambda^{\mathrm{Re}}_\theta(\theta) - \mathrm{i}\Lambda^{\mathrm{Im}}_\theta(\theta)\\
&\Sigma^{\mathrm{I}}_{\alpha\beta}(\theta) = \overline{\Sigma^{\mathrm{II}}_{\alpha\beta}(\theta)} = \Sigma^{\mathrm{Re}}_{\alpha\beta}(\theta) - \mathrm{i}\Sigma^{\mathrm{Im}}_{\alpha\beta}(\theta)\\
&s_1 = \overline{s_2} = s_{\mathrm{Re}} + \mathrm{i}s_{\mathrm{Im}}\\
&K_{\mathrm{I}} = \overline{K_{\mathrm{II}}} = \frac{K_{\mathrm{Re}} + \mathrm{i}K_{\mathrm{Im}}}{2\sqrt{2\pi}}
\end{aligned} \tag{29}$$

where $\mathrm{i} = \sqrt{-1}$. Substituting these expressions into Eq. (27), we have

$$\begin{aligned}
u(r,\theta_k) =& \frac{1}{\sqrt{2\pi}} r^{s_{\mathrm{Re}}} K_{\mathrm{Re}}[\Lambda^{\mathrm{Re}}_r(\theta_k)\cos(s_{\mathrm{Im}}\ln r) + \Lambda^{\mathrm{Im}}_r(\theta_k)\sin(s_{\mathrm{Im}}\ln r)]\\
&- \frac{1}{\sqrt{2\pi}} r^{s_{\mathrm{Re}}} K_{\mathrm{Im}}[\Lambda^{\mathrm{Re}}_r(\theta_k)\sin(s_{\mathrm{Im}}\ln r) - \Lambda^{\mathrm{Im}}_r(\theta_k)\cos(s_{\mathrm{Im}}\ln r)]\\
w(r,\theta_k) =& \frac{1}{\sqrt{2\pi}} r^{s_{\mathrm{Re}}} K_{\mathrm{Re}}[\Lambda^{\mathrm{Re}}_\theta(\theta_k)\cos(s_{\mathrm{Im}}\ln r) + \Lambda^{\mathrm{Im}}_\theta(\theta_k)\sin(s_{\mathrm{Im}}\ln r)]\\
&- \frac{1}{\sqrt{2\pi}} r^{s_{\mathrm{Re}}} K_{\mathrm{Im}}[\Lambda^{\mathrm{Re}}_\theta(\theta_k)\sin(s_{\mathrm{Im}}\ln r) - \Lambda^{\mathrm{Im}}_\theta(\theta_k)\cos(s_{\mathrm{Im}}\ln r)]
\end{aligned} \tag{30}$$

In the same way, the discrete singular stress fields are readily derived

$$\begin{aligned}
\sigma_{\alpha\beta}(r,\theta_k) =& \frac{1}{\sqrt{2\pi}} r^{s_{\mathrm{Re}}-1} K_{\mathrm{Re}}[\Sigma^{\mathrm{Re}}_{\alpha\beta}(\theta_k)\cos(s_{\mathrm{Im}}\ln r) + \Sigma^{\mathrm{Im}}_{\alpha\beta}(\theta_k)\sin(s_{\mathrm{Im}}\ln r)]\\
&- \frac{1}{\sqrt{2\pi}} r^{s_{\mathrm{Re}}-1} K_{\mathrm{Im}}[\Sigma^{\mathrm{Re}}_{\alpha\beta}(\theta_k)\sin(s_{\mathrm{Im}}\ln r) - \Sigma^{\mathrm{Im}}_{\alpha\beta}(\theta_k)\cos(s_{\mathrm{Im}}\ln r)]
\end{aligned} \tag{31}$$

Similar to the case with two real singularities, the complete displacement and singular stress fields can be obtained by means of the interpolation method. In addition, the angular variations of displacement and stress components relate to the computed eigenvectors through Eqs. (14) and (16), respectively. Prior to

comparing with the analytical solutions, the numerical angular variations of displacement and singular stress fields should be normalized by a specified identical rule.

4. Numerical results and discussions

In this section, the convergence, accuracy and efficiency characteristics of the proposed boundary value method for determining the singular behavior of the stress field in the vicinity of the singular point is verified, where the isotropic metal materials Nickel and Aluminum are regarded to be the material 1 and 2 of the bimaterial system respectively. The relevant material properties are $E_1 = 210$ GPa, $v_1 = 0.31$ and $E_2 = 68.9$ GPa, $v_2 = 0.25$. In the implementation of numerical simulation, the scattered meshless points are uniformly distributed in material 1 and 2 of the bimaterial system with n_1 and n_2 denoting the point number of the respective material. Furthermore unless specifically stated, the boundary conditions prescribed on the two wedge-side surfaces are both set to be *Traction-free*.

4.1. Interface crack

The interface crack problem with the bonded interface along $\theta = 0°$ is first analyzed numerically based on the same point distribution, i.e. $n_1 = n_2$. The exact solutions of the order of stress singularity are $0.5 \pm i0.0603$ for plane strain and $0.5 \pm i0.0636$ for plane stress. The variations of the computed orders of stress singularity with the point number n_1 or n_2 are shown in Fig. 2. It is obvious that the numerical results exhibit strong and monotonic convergence toward the exact solutions with increasing the number of scattered points. When the point number n_1 or n_2 reaches to 51, the numerical results are $0.4984 + i0.0603$ for plane strain and $0.4985 + i0.0637$ for plane stress, which are well agreement with the exact solutions. On the basis of the results shown in Fig. 2, it is can be concluded that the present developed numerical method on determining the orders of stress singularity has high accuracy and quick convergence characteristics.

In addition, the angular variations of displacement and singular stress fields are also investigated. The asymptotic expressions of the analytical displacement and singular stress fields are of the forms

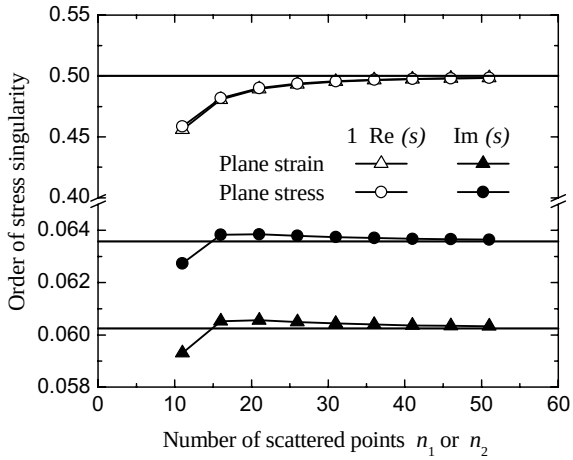

Fig. 2. Convergence of the orders of stress singularity for interface crack problem.

$$u_\alpha = \sqrt{\frac{1}{2\pi}}\left[\mathrm{Re}(Kr^{i\varepsilon})\Lambda^{\mathrm{I}}_\alpha(\theta,\varepsilon,\nu_j,\mu_j) + \mathrm{Im}(Kr^{i\varepsilon})\Lambda^{\mathrm{II}}_\alpha(\theta,\varepsilon,\nu_j,\mu_j)\right] \quad (j=1,2)$$
$$\sigma_{\alpha\beta} = \frac{1}{\sqrt{2\pi r}}\left[\mathrm{Re}(Kr^{i\varepsilon})\Sigma^{\mathrm{I}}_{\alpha\beta}(\theta,\varepsilon) + \mathrm{Im}(Kr^{i\varepsilon})\Sigma^{\mathrm{II}}_{\alpha\beta}(\theta,\varepsilon)\right] \quad (\alpha,\beta = r,\theta) \tag{32}$$

and

$$K = K_{\mathrm{I}} + iK_{\mathrm{II}} \quad \varepsilon = \frac{1}{2\pi}\ln\left(\frac{\mu_1 + \mu_2\kappa_1}{\mu_2 + \mu_1\kappa_2}\right) \tag{33}$$

where $\kappa_j = 3 - 4\nu_j$ for plane strain and $\kappa_j = (3-\nu_j)/(1+\nu_j)$ for stain stress with the subscript j referring to the dissimilar materials. The explicit analytical expressions of the angular variations of singular stress field are given by Rice et al. (1990) and those of displacement field are presented in the Appendix C. The displacement and singular stress fields can also be rewritten into the real forms as

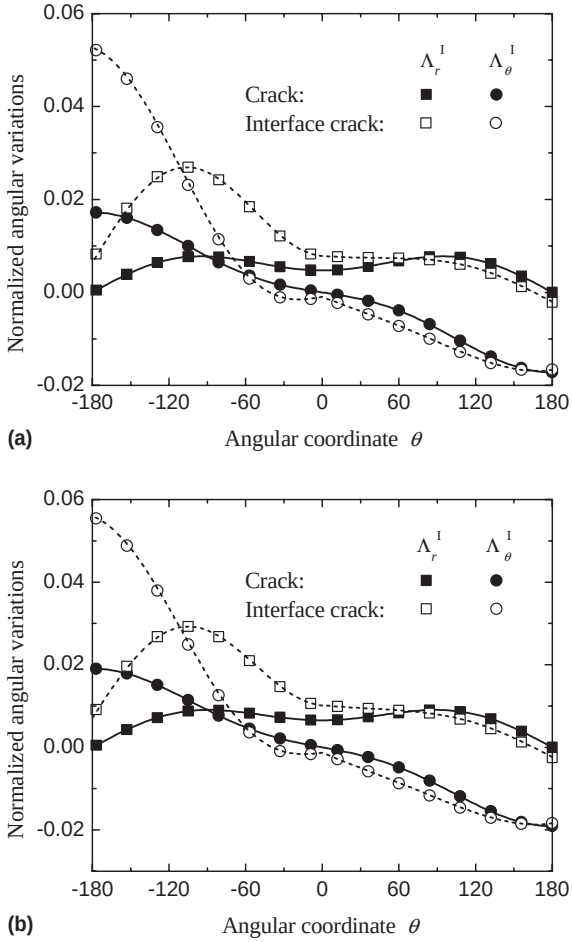

Fig. 3. Normalized displacement angular variations for pure Mode I loading of a crack and an interface crack: (a) plane strain; (b) plane stress.

$$
\begin{aligned}
u_\alpha &= \sqrt{\frac{r}{2\pi}} K_{\mathrm{I}} \left[\Lambda_\alpha^{\mathrm{I}}(\theta, \varepsilon, \nu_j, \mu_j) \cos(\varepsilon \ln r) + \Lambda_\alpha^{\mathrm{II}}(\theta, \varepsilon, \nu_j, \mu_j) \sin(\varepsilon \ln r) \right] \\
&\quad - \sqrt{\frac{r}{2\pi}} K_{\mathrm{II}} \left[\Lambda_\alpha^{\mathrm{I}}(\theta, \varepsilon, \nu_j, \mu_j) \sin(\varepsilon \ln r) - \Lambda_\alpha^{\mathrm{II}}(\theta, \varepsilon, \nu_j, \mu_j) \cos(\varepsilon \ln r) \right] \\
\sigma_{\alpha\beta} &= \frac{1}{\sqrt{2\pi r}} K_{\mathrm{I}} \left[\Sigma_{\alpha\beta}^{\mathrm{I}}(\theta, \varepsilon) \cos(\varepsilon \ln r) + \Sigma_{\alpha\beta}^{\mathrm{II}}(\theta, \varepsilon) \sin(\varepsilon \ln r) \right] \\
&\quad - \frac{1}{\sqrt{2\pi r}} K_{\mathrm{II}} \left[\Sigma_{\alpha\beta}^{\mathrm{I}}(\theta, \varepsilon) \sin(\varepsilon \ln r) - \Sigma_{\alpha\beta}^{\mathrm{II}}(\theta, \varepsilon) \cos(\varepsilon \ln r) \right]
\end{aligned}
\tag{34}
$$

Note that Eq. (33) has the same forms as Eqs. (30) and (31) provided that the following equivalence relations

$$
s_{\mathrm{Re}} + \mathrm{i} s_{\mathrm{Im}} \Longleftrightarrow 0.5 + \mathrm{i}\varepsilon \quad \mathrm{Re} + \mathrm{i}\,\mathrm{Im} \Longleftrightarrow \mathrm{I} + \mathrm{i}\,\mathrm{II} \tag{35}
$$

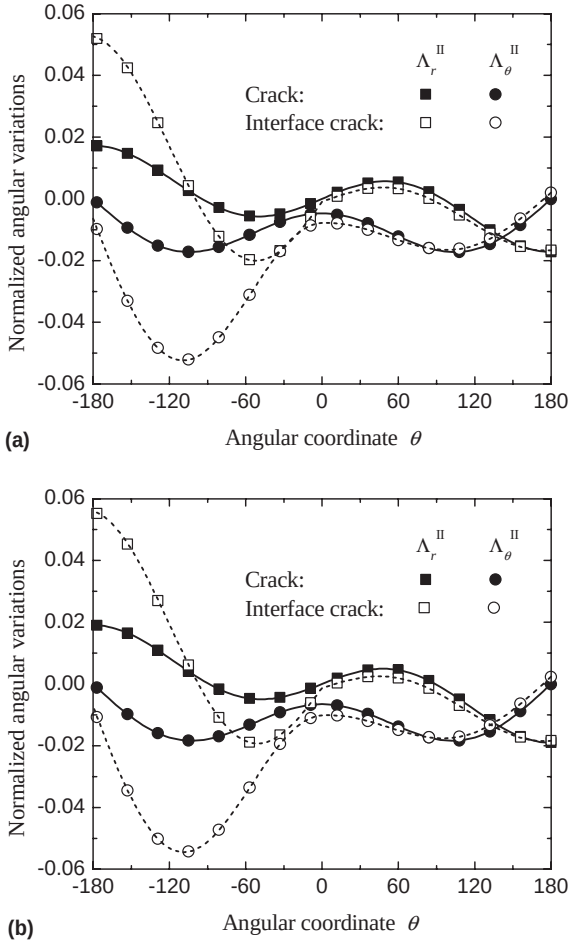

Fig. 4. Normalized displacement angular variations for pure Mode II loading of a crack and an interface crack: (a) plane strain; (b) plane stress.

are considered. In other words, the real part corresponds to the mode I and imaginary part to the mode II. If the bonded dissimilar materials have the same elasticity, we find $\varepsilon = 0$ and the interface crack problem reduces to the well-known crack problem in a homogeneous isotropic material.

The numerical results of the angular variations of the displacement and singular stress fields are obtained on the basis of the eigenvectors associated with the physically admissible eigenvalues ($n_1 = n_2 = 51$). The normalized rule for the interface crack problem is set to be $\Sigma_\theta^{\mathrm{Re}}(0) + \mathrm{i}\Sigma_\theta^{\mathrm{Im}}(0) = 1$, which is identical to $\Sigma_{r\theta}^{\mathrm{Re}}(0) + \mathrm{i}\Sigma_{r\theta}^{\mathrm{Im}}(0) = 1$. While for the crack problem, the rule reduces to be $\Sigma_\theta^{\mathrm{I}}(0) = \Sigma_{r\theta}^{\mathrm{II}}(0) = 1$. The comparisons of the normalized numerical results with the exact solutions are plotted against with the angular coordinate θ in Figs. 3–6. The solid symbols and continuous lines denote the numerical results and exact solutions of the well-known crack problem respectively. The hollow symbols and the dashed lines denote the numerical results and exact solutions of the interface crack problem respectively. It is clear that the numerical results are coincident with the exact solutions, and 51 scattered points uniformly distributed in each domain of bimaterial systems are enough to achieve high accuracy. This technique of point

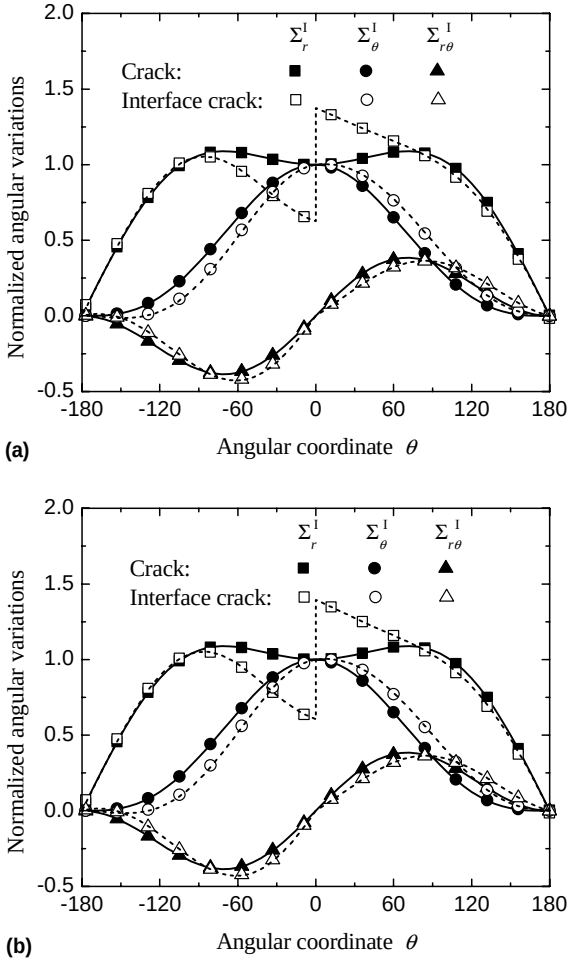

Fig. 5. Normalized stress angular variations for pure Mode I loading of a crack and an interface crack: (a) plane strain; (b) plane stress.

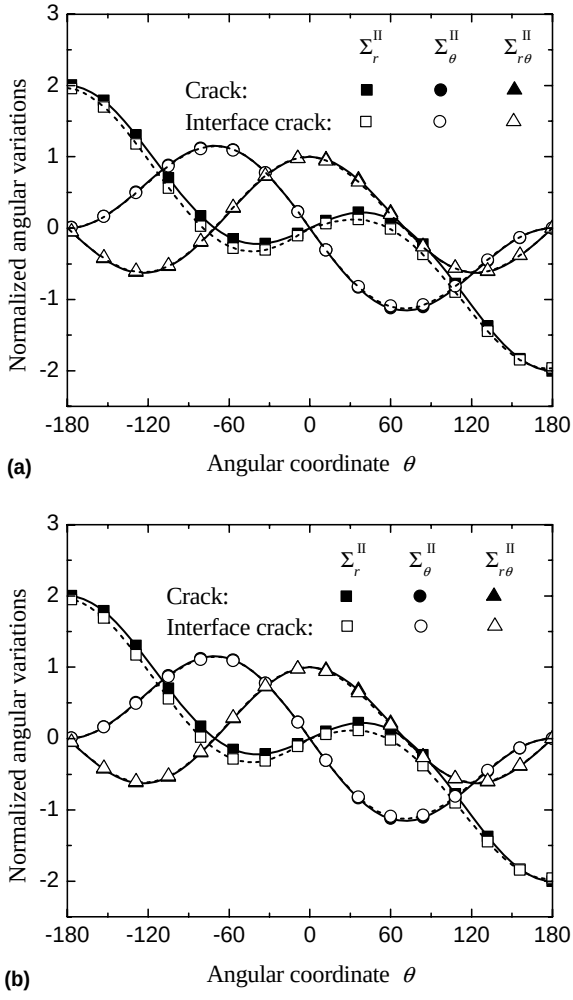

Fig. 6. Normalized stress angular variations for pure Mode II loading of a crack and an interface crack: (a) plane strain; (b) plane stress.

Table 1
The orders of stress singularity for the common bimaterial wedges with various boundary condition combinations

$\pm\theta$	State	Mode	Numerical results	Exact solutions
150°	Plane strain	Mode I	0.4508	0.4517
		Mode II	0.3102	0.3115
	Plane stress	Mode I	0.4462	0.4470
		Mode II	0.3151	0.3163
170°	Plane strain	Oscillatory	$0.4676 \pm i0.0571$	$0.4691 \pm i0.0572$
	Plane stress	Oscillatory	$0.4677 \pm i0.0610$	$0.4691 \pm i0.0611$

distribution will be used in the following numerical analysis unless otherwise stated. By now, we reach the conclusion that the present numerical method can efficiently determine the two important parameters, the

order of the stress singularity and the associated angular variations, of the asymptotic displacement and singular stress fields. In the following, we will use this method to study the singular behavior of common bimaterial wedge and junctions. In addition, from the Figs. 5(a) and (b) we find that the angular variations of mode I normal stress along the radial direction are discontinuous at the interface. The absolute quantity of the jump relates only to the parameter ε by $|4\tanh(\varepsilon\pi)|$.

4.2. Bimaterial wedge

In this subsection, the ability for determining the angular variations of the common bimaterial wedges is examined first. The two selected analytical models are A with wedge angle $\theta_1 = -\theta_2 = 150°$ and B with $\theta_1 = -\theta_2 = 170°$. From the exact and numerical results presented in Table 1 we know that the model A has two real stress singularities and model B has oscillatory stress singularity. The computed orders of stress singularity for different deformation modes are all well agreement with the relevant exact solutions. In the meantime, the normalized angular variations of displacement and singular stress fields are easily obtained,

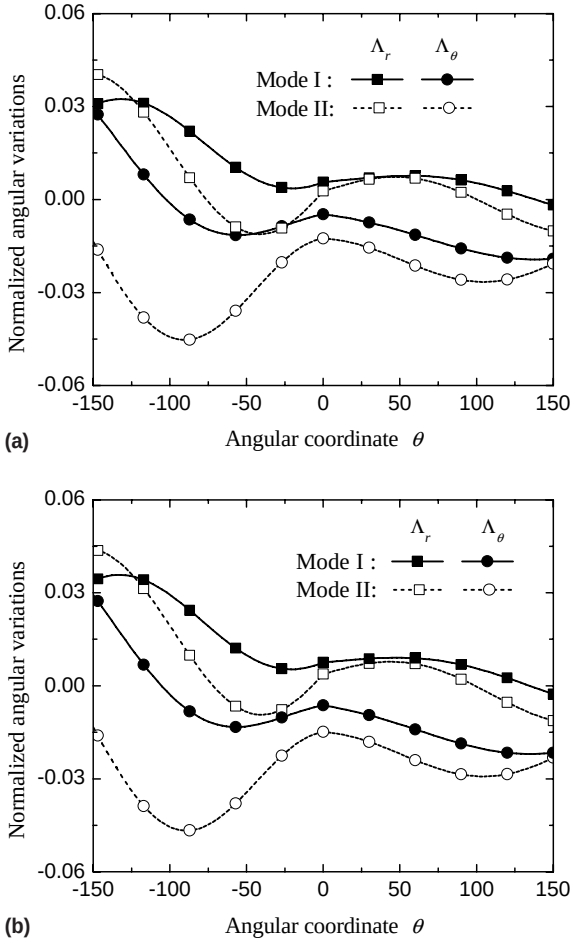

Fig. 7. Normalized displacement angular variations of a common bimaterial wedge with two real stress singularities: (a) plane strain; (b) plane stress.

where the normalized rule is set to be $\Sigma_{\theta}^{\mathrm{I}}(0) = \Sigma_{r\theta}^{\mathrm{II}}(0) = 1$ for model A and $\Sigma_{\theta}^{\mathrm{I}}(0) + \mathrm{i}\Sigma_{\theta}^{\mathrm{II}}(0) = 1$ for mode B. The computed angular variations against with the angular coordinate θ for model A are depicted in Figs. 7 and 8, and for model B are depicted in Figs. 9 and 10. The solid symbols and lines in the Figures denote the results of mode I, while the hollow symbols and the dashed lines denote the results for mode II. It can be seen from the Figures that at the interface both $\Sigma_r^{\mathrm{I}}(\theta)$ and $\Sigma_r^{\mathrm{II}}(\theta)$ are discontinuous for model A, but only $\Sigma_r^{\mathrm{I}}(\theta)$ is discontinuous for model B. The $\Sigma_r^{\mathrm{I}}(\theta)$ is coupled with $\Sigma_r^{\mathrm{II}}(\theta)$ at two wedge-side surfaces even though on which the *Traction-free* boundary conditions are prescribed. In addition, we cannot find a direction along which the both deformation modes of $\Sigma_{\theta}(\theta)$ and $\Sigma_{r\theta}(\theta)$ are decoupled each other. All of these are the particular new features of the common bimaterial wedge comparing with the well-known crack and interface crack problems.

Furthermore, four special cases of the bimaterial wedges, namely a right angle ($\theta_1 = -\theta_2 = 45°$), a half plane ($\theta_1 = -\theta_2 = 90°$), a right-angled corner ($\theta_1 = 90°$ and $\theta_2 = -180°$) and an interface crack ($\theta_1 = -\theta_2 = 180°$) which are of very interest in engineering, are considered to study the effects of various

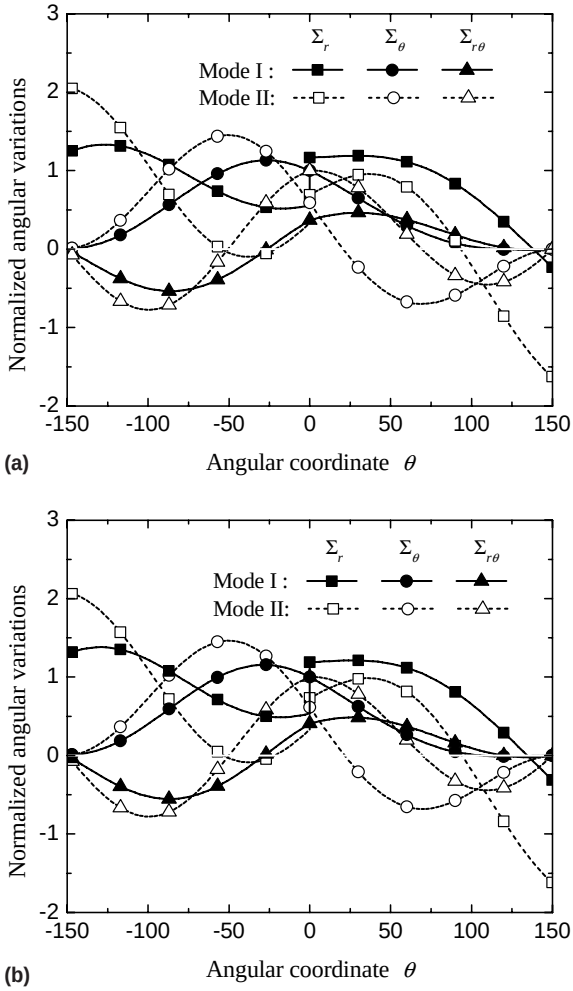

Fig. 8. Normalized stress angular variations of a common bimaterial wedge with two real stress singularities: (a) plane strain; (b) plane stress.

boundary conditions to the stress singularity. Table 2 shows the order of stress singularities corresponding to four physically admissible boundary condition combinations. It is found that the oscillatory stress singularities of an interface crack with mixed boundary conditions TD and DT are weaker than those with homogeneous boundary conditions TT and DD. For the right-angled corner, there are single and two real stress singularities for the mixed and homogeneous boundary conditions respectively. In the case of a half plane, oscillatory stress singularity is found for DT and no stress singularity is found for TD. Finally for the right angle wedge, the stress singularity exists only for mixed boundary condition DT. The comparisons of the results presented in Table 2 indicate that the various combinations of boundary conditions do have a significant influence on the number and strength of the stress singularity.

4.3. Bimaterial junction

A fully bonded nickel–aluminum bimaterial junction in plane strain is considered in Fig. 11 for varying wedge angle θ_1 with respect to material 1. It can be seen that there are two real singularities in the regions

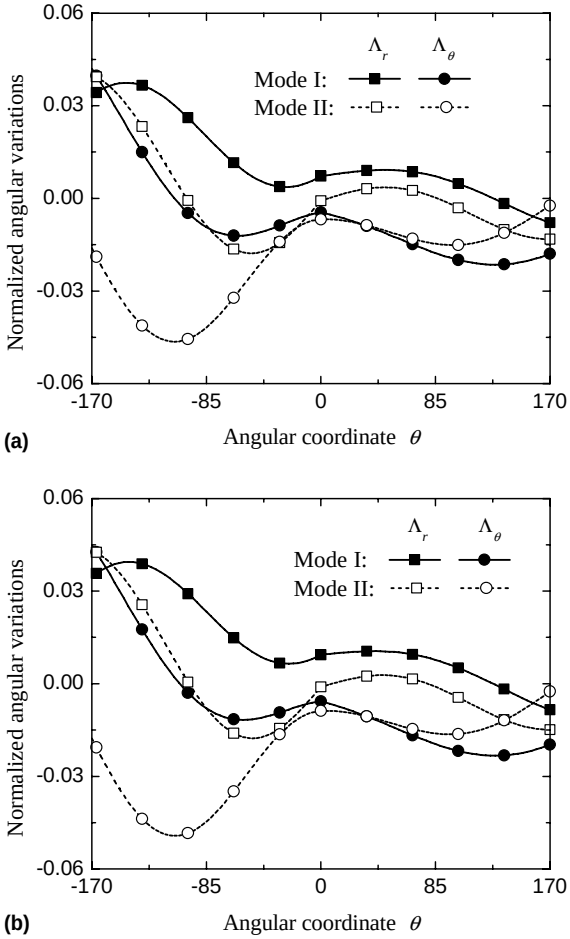

Fig. 9. Normalized displacement angular variations of a common bimaterial wedge with oscillatory stress singularity: (a) plane strain; (b) plane stress.

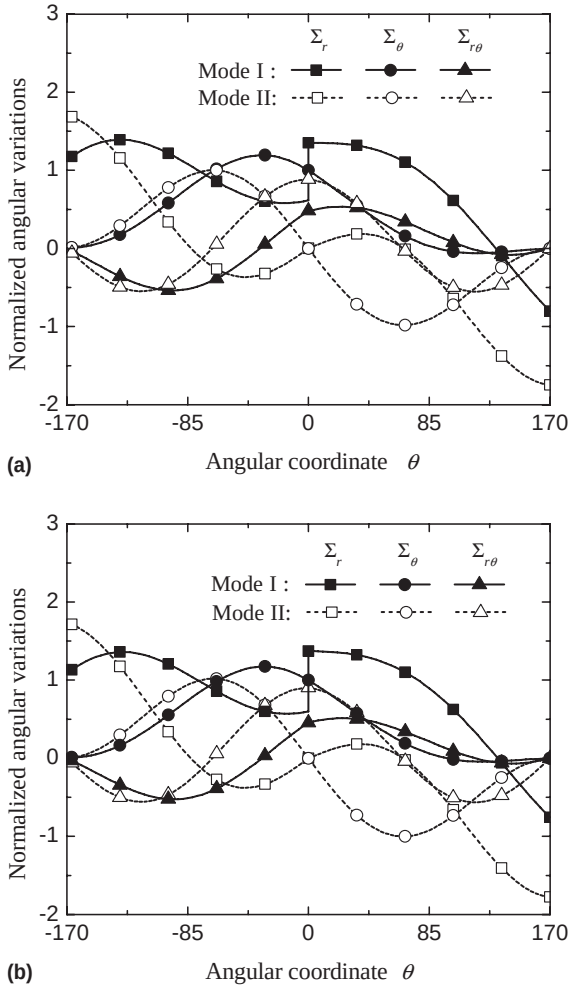

Fig. 10. Normalized stress angular variations of a common bimaterial wedge with oscillatory stress singularity: (a) plane strain; (b) plane stress.

Table 2
The orders of stress singularities for a right angle wedge, a half plane, a right-angled corner and an interface crack

Cases	Right angle	Half plane	Right-angled corner	Interface crack
TT	–	0.0601	0.4980 0.2306	$0.4989 \pm i0.0603$
DD	–	0.1732	0.3593 0.1091	$0.4988 \pm i0.0401$
TD	–	–	0.0793 –	$0.1672 \pm i0.0252$
DT	0.0788	$0.3348 \pm i0.1099$	0.2072 –	$0.3316 \pm i0.0754$

$90° < \theta_1 < 180°$ and $262.5° \leqslant \theta_1 \leqslant 270°$, and only one real singularity in the region $180° < \theta_1 < 262.5°$. When $\theta_1 = 180°$, no singularity is found. The singularities for this kind of model are much weaker than the classical inverse square root singularity. On the other hand, a debonded nickel–aluminum bimaterial junction in plane strain is considered in Fig. 12 for varying wedge angle θ_1. Note that the singularity be-

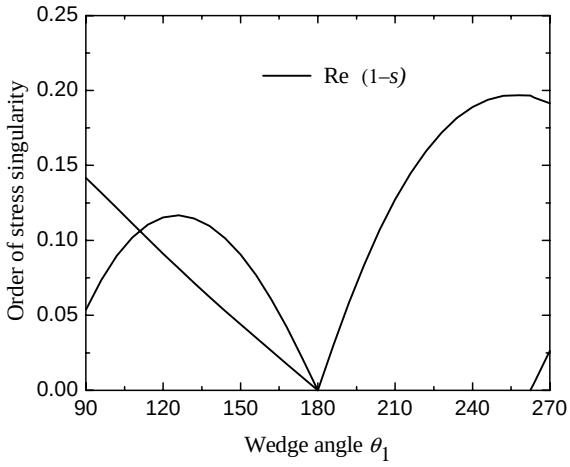

Fig. 11. Orders of stress singularity for a fully bonded bimaterial junction.

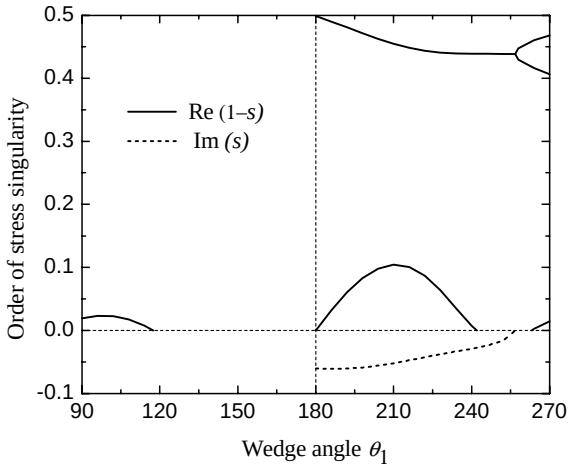

Fig. 12. Orders of stress singularity for a debonded bimaterial junction.

comes very complex and one to three stress singularities are found due to the presence of a crack between two dissimilar materials. It is very interesting that there are one real and a couple of conjugate complex singularities when θ_1 is larger than 180° and less than 240°, and three real singularities in a small region near 270°.

Furthermore, the normalized angular variations of displacement and singular stress fields are shown in Figs. 13 and 14 corresponding to the debonded bimaterial junction ($\theta_1 = 210°$) with one real and a couple of conjugate complex eigenvalues. The deformation of mode I corresponds to the real part of the oscillatory singularity (0.4548), mode II corresponds to the imaginary part of the oscillatory singularity (0.0521), and mode III corresponds to the real singularity (0.1042). The normalized angular variations associated with modes I, II and III are denoted by the solid, dashed and dotted continuous lines respectively. The normalized rules used here are the maximum of the modulus $\max \|\Sigma^{\mathrm{I}}_{\alpha\beta}(\theta) + \mathrm{i}\Sigma^{\mathrm{II}}_{\alpha\beta}(\theta)\| = 1$ for oscillatory singularity and the maximum of the absolute value $\max \mid \Sigma^{\mathrm{III}}_{\alpha\beta}(\theta) \mid = 1$ for the real singularity.

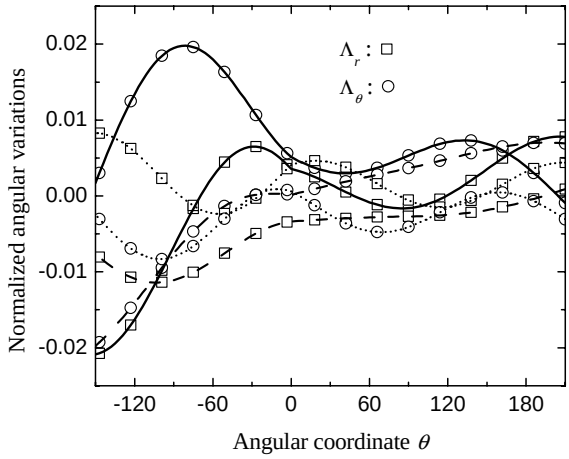

Fig. 13. Normalized displacement angular variations of a debonded bimaterial junction with one real and a couple of complex stress singularity.

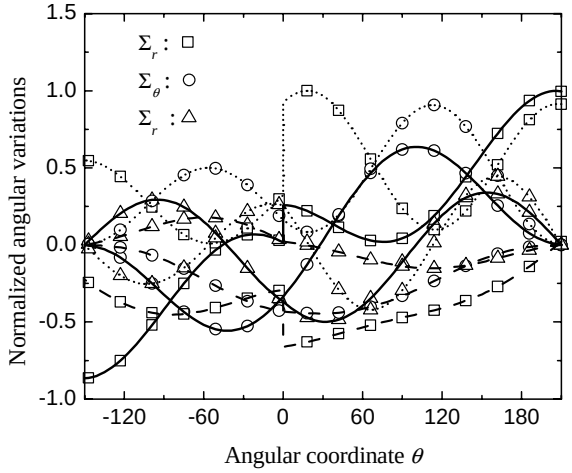

Fig. 14. Normalized stress angular variations of a debonded bimaterial junction with one real and a couple of complex stress singularity.

5. Conclusions

A novel boundary value method for investigating the singular behavior of bimaterial systems is developed based on the governing equations of linear elasticity and the eigenfunction expansion technique. Discretizing the resulted formulations by using of the finite cloud method, we obtain the standard eigenproblem in singular eigenvalue. The characteristic matrix equation is then solved numerically by the LAPACK subroutine to obtain the physically admissible eigenvalues and the associated eigenvectors. Two benchmark problems, the well-known crack and interface crack, are analyzed to validate the present proposed numerical method. The calculated orders of stress singularity exhibit strong and monotonic con-

vergence toward the exact solutions with increasing the number of scattered points, and the convergent results show very good agreement between the boundary value method and the exact solutions. Subsequently, this powerful method is successfully used to study the singular behavior of the common bimaterial systems. The significant influence of various boundary conditions on both the number and strength of the stress singularity is also verified.

Compared to the analytical approaches and finite element methods, the developed boundary value procedure originated from the equilibrium equations is more powerful and wieldy for the study of stress singularity of the composites with complex geometrical configurations.

Acknowledgements

The work given in this paper is sponsored both by the Scientific Research Foundation for the Returned Overseas Chinese Scholars of Zhejiang Province and by Zhejiang University of Technology. The author is grateful the reviewers for the valuable comments.

Appendix A

$$[\mathbf{A}_{uu}]_{kj} = (\lambda + 2\mu)N_j(\theta_k) \tag{A.1}$$

$$[\mathbf{A}_{ww}]_{kj} = \mu N_j(\theta_k) \tag{A.2}$$

$$[\mathbf{B}_{uw}]_{kj} = (\lambda + \mu)N'_j(\theta_k) \tag{A.3}$$

$$[\mathbf{B}_{wu}]_{kj} = (\lambda + \mu)N'_j(\theta_k) \tag{A.4}$$

$$[\mathbf{A}_{uw}]_{kj} = [\mathbf{A}_{wu}]_{kj} = [\mathbf{B}_{uu}]_{kj} = [\mathbf{B}_{ww}]_{kj} = 0 \tag{A.5}$$

$$[\mathbf{C}_{uu}]_{kj} = \mu N''_j(\theta_k) - (\lambda + 2\mu)N_j(\theta_k) \tag{A.6}$$

$$[\mathbf{C}_{uw}]_{kj} = -(\lambda + 3\mu)N'_j(\theta_k) \tag{A.7}$$

$$[\mathbf{C}_{wu}]_{kj} = (\lambda + 3\mu)N'_j(\theta_k) \tag{A.8}$$

$$[\mathbf{C}_{ww}]_{kj} = (\lambda + 2\mu)N''_j(\theta_k) - \mu N_j(\theta_k) \tag{A.9}$$

Appendix B

$$[\mathbf{b}_{uu}]_j = \lambda N_j(\theta) \tag{B.1}$$

$$[\mathbf{b}_{ww}]_j = \mu N_j(\theta) \tag{B.2}$$

$$[\mathbf{c}_{uu}]_j = (\lambda + 2\mu)N_j(\theta) \tag{B.3}$$

$$[\mathbf{c}_{uw}]_j = (\lambda + 2\mu)N'_j(\theta) \tag{B.4}$$

$$[\mathbf{c}_{wu}]_j = \mu N'_j(\theta) \tag{B.5}$$

$$[\mathbf{c}_{ww}]_j = -\mu N_j(\theta) \tag{B.6}$$

Appendix C

Listed below are the angular variations of the displacement field in the tip of an interface crack for mode I and mode II deformations

$$\Lambda_r^{\mathrm{I}} = \alpha_j\left[\kappa_j\left(\cos\frac{\theta}{2} + 2\varepsilon\sin\frac{\theta}{2}\right) - \beta_j\left(\cos\frac{3\theta}{2} + 2\varepsilon\sin\frac{3\theta}{2}\right) - (1+4\varepsilon^2)\sin\theta\sin\frac{\theta}{2}\right] \tag{C.1}$$

$$\Lambda_\theta^{\mathrm{I}} = \alpha_j\left[\kappa_j\left(-\sin\frac{\theta}{2} + 2\varepsilon\cos\frac{\theta}{2}\right) + \beta_j\left(\sin\frac{3\theta}{2} - 2\varepsilon\cos\frac{3\theta}{2}\right) - (1+4\varepsilon^2)\sin\theta\cos\frac{\theta}{2}\right] \tag{C.2}$$

$$\Lambda_r^{\mathrm{II}} = \alpha_j\left[\kappa_j\left(-\sin\frac{\theta}{2} + 2\varepsilon\cos\frac{\theta}{2}\right) + \beta_j\left(\sin\frac{3\theta}{2} - 2\varepsilon\cos\frac{3\theta}{2}\right) + (1+4\varepsilon^2)\sin\theta\cos\frac{\theta}{2}\right] \tag{C.3}$$

$$\Lambda_\theta^{\mathrm{II}} = \alpha_j\left[-\kappa_j\left(\cos\frac{\theta}{2} + 2\varepsilon\sin\frac{\theta}{2}\right) + \beta_j\left(\cos\frac{3\theta}{2} + 2\varepsilon\sin\frac{3\theta}{2}\right) - (1+4\varepsilon^2)\sin\theta\sin\frac{\theta}{2}\right] \tag{C.4}$$

where

$$\alpha_1 = \frac{\mathrm{e}^{-\varepsilon(\pi-\theta)}}{(1+4\varepsilon^2)\cosh(\pi\varepsilon)} \tag{C.5}$$

$$\alpha_2 = \frac{\mathrm{e}^{\varepsilon(\pi+\theta)}}{(1+4\varepsilon^2)\cosh(\pi\varepsilon)} \tag{C.6}$$

$$\beta_1 = \mathrm{e}^{2\varepsilon(\pi-\theta)} \tag{C.7}$$

$$\beta_2 = \mathrm{e}^{-2\varepsilon(\pi+\theta)} \tag{C.8}$$

The subscripts 1 and 2 denote the materials 1 and 2 respectively. If the parameter ε is equal to zero, the angular variations for the well-known crack problem are obtained.

References

Aluru, N.R., Li, G., 2001. Finite cloud method: a true meshless technique based on a fixed reproducing kernel approximation. International Journal for Numerical Methods in Engineering 50, 2373–2410.

Bazant, Z.P., Estenssoro, L.F., 1979. Surface singularity and crack propagation. International Journal of Solids and Structures 15, 405–426.

Bogy, D.B., 1971. Two edge-bonded elastic wedges of different materials and wedge angles under surface tractions. ASME Journal of Applied Mechanics 38, 377–386.

Bogy, D.B., Wang, K.C., 1971. Stress singularities at interface corners in bonded dissimilar isotropic elastic materials. International Journal of Solids and Structures 7, 993–1005.

Chen, D.H., Nisitani, H., 1993. Singular stress field near the corner of jointed dissimilar materials. ASME Journal of Applied Mechanics 60, 607–613.

Chen, B.J., Xiao, Z.M., Liew, K.M., 2002. A screw dislocation in a piezoelectric bi-material wedge. International Journal of Engineering Science 40, 1665–1685.

Chen, B.J., Xiao, Z.M., Liew, K.M., 2003. A piezoelectric screw dislocation near a wedge-shaped bi-material interface. International Journal of Solids and Structures 40, 2041–2056.

Chen, B.J., Xiao, Z.M., Liew, K.M., 2004. A line dislocation interacting with a semi-infinite crack in piezoelectric solid. International Journal of Engineering Science 42, 1–11.

Ghahremani, F., 1991. A numerical variational method for extracting 3D singularities. International Journal of Solids and Structures 27, 1371–1386.

Gu, L., Belytschko, T., 1994. A numerical study of stress singularities in a two-material wedge. International Journal of Solids and Structures 31, 865–889.

Liang, J., Liew, K.M., 2001. Boundary elements for half-space problems via fundamental solutions: a three-dimensional analysis. International Journal for Numerical Methods in Engineering 52, 1189–1202.

Liew, K.M., Liang, J., 2002. Modeling of 3D transversely piezoelectric and elastic bimaterials using the boundary element method. Computational Mechanics 29, 151–162.

Liew, K.M., Liang, J., 2003. Three-dimensional piezoelectric boundary element analysis of transversely isotropic half-space. Computational Mechanics 32, 29–39.

Pageau, S.S., Joseph, P.F., Biggers, S.B., 1995. Finite element analysis of anisotropic materials with singular inplane stress fields. International Journal of Solids and Structures 32, 571–591.

Rice, J.R., Suo, Z.G., Wang, J.S., 1990. Mechanics and thermodynamics of brittle interfacial failure in bimaterial systems. In: Rühle, M. (Ed.), Metal–Ceramic Interfaces. Pergamon Press, New York, pp. 269–294.

Somaratna, N., Ting, T.C.T., 1986. Three-dimensional stress singularities in anisotropic materials and composites. International Journal of Engineering Science 24, 1115–1134.

Sze, K.Y., Wang, H.T., 2000. A simple finite element formulation for computing stress singularities at bimaterial interfaces. Finite Element in Analysis and Design 35, 97–118.

Williams, M.L., 1959. The stress around a fault or crack in dissimilar media. Bulletin of the Seismological Society of America 49, 199–204.

Xu, J.Q., Liu, Y.H., Wang, X.G., 1999. Numerical methods for the determination of multiple stress singularities and related stress intensity coefficients. Engineering Fracture Mechanics 63, 775–790.

Xu, J.Q., Wang, X.G., Yoshiharu, M., 2001. Stress intensity factors of a surface crack near an interface end. International Journal of Fracture 111, 251–264.

Yamada, Y., Okumura, H., 1983. Finite element analysis of stress and strain singularity eigenstate in inhomogeneous media or composite materials. In: Atluri, S.N. (Ed.), Hybrid and Mixed Finite Element Methods. John Wiley, New York, pp. 325–343.